

Observation of muon neutrino disappearance with the MINOS detectors in the NuMI neutrino beam

D. G. Michael,^{5,*} P. Adamson,^{11,21,30} T. Alexopoulos,³⁶ W. W. M. Allison,²⁴ G. J. Alner,²⁶ K. Anderson,¹¹ C. Andreopoulos,^{26,2} M. Andrews,¹¹ R. Andrews,¹¹ K. E. Arms,²² R. Armstrong,¹⁴ C. Arroyo,²⁹ D. J. Auty,³⁰ S. Avvakumov,²⁹ D. S. Ayres,¹ B. Baller,¹¹ B. Barish,⁵ M. A. Barker,²⁴ P. D. Barnes Jr.,²⁰ G. Barr,²⁴ W. L. Barrett,³⁴ E. Beall,^{1,22} B. R. Becker,²² A. Belias,²⁶ T. Bergfeld,²⁸ R. H. Bernstein,¹¹ D. Bhattacharya,²⁵ M. Bishai,⁴ A. Blake,⁶ V. Bocean,¹¹ B. Bock,²³ G. J. Bock,¹¹ J. Boehm,¹² D. J. Boehnlein,¹¹ D. Bogert,¹¹ P. M. Border,²² C. Bower,¹⁴ S. Boyd,²⁵ E. Buckley-Geer,¹¹ C. Bungau,³⁰ A. Byon-Wagner,¹¹ A. Cabrera,²⁴ J. D. Chapman,⁶ T. R. Chase,²² D. Cherdack,³³ S. K. Chernichenko,¹⁵ S. Childress,¹¹ B. C. Choudhary,^{11,5} J. H. Cobb,²⁴ J. D. Cossairt,¹¹ H. Courant,²² D. A. Crane,¹ A. J. Culling,⁶ J. W. Dawson,¹ J. K. de Jong,¹³ D. M. DeMuth,²² A. De Santo,²⁴ M. Dierckxsens,⁴ M. V. Diwan,⁴ M. Dorman,^{21,26} G. Drake,¹ D. Drakoulakos,² R. Ducar,¹¹ T. Durkin,²⁶ A. R. Erwin,³⁶ C. O. Escobar,⁷ J. J. Evans,²⁴ O. D. Fackler,²⁰ E. Falk Harris,³⁰ G. J. Feldman,¹² N. Felt,¹² T. H. Fields,¹ R. Ford,¹¹ M. V. Frohne,³ H. R. Gallagher,^{33,24,1,22} M. Gebhard,¹⁴ G. A. Giurgiu,¹ A. Godley,²⁸ J. Gogos,²² M. C. Goodman,¹ Yu. Gornushkin,¹⁸ P. Gouffon,²⁷ R. Gran,²³ E. Grashorn,^{22,23} N. Grossman,¹¹ J. J. Grudzinski,¹ K. Grzelak,²⁴ V. Guarino,¹ A. Habig,²³ R. Halsall,²⁶ J. Hanson,⁵ D. Harris,¹¹ P. G. Harris,³⁰ J. Hartnell,^{26,24} E. P. Hartouni,²⁰ R. Hatcher,¹¹ K. Heller,²² N. Hill,¹ Y. Ho,¹⁰ A. Holin,²¹ C. Howcroft,^{5,6} J. Hysten,¹¹ M. Ignatenko,¹⁸ D. Indurthy,³² G. M. Irwin,²⁹ M. Ishitsuka,¹⁴ D. E. Jaffe,¹² C. James,¹¹ L. Jenner,²¹ D. Jensen,¹¹ T. Joffe-Minor,¹ T. Kafka,³³ H. J. Kang,²⁹ S. M. S. Kasahara,²² J. Kilmer,¹¹ H. Kim,⁵ M. S. Kim,²⁵ G. Koizumi,¹¹ S. Kopp,³² M. Kordosky,^{21,32} D. J. Koskinen,^{21,23} M. Kostin,³² S.K. Kotelnikov,¹⁹ D. A. Krakauer,¹ A. Kreymer,¹¹ S. Kumaratunga,²² A. S. Ladran,²⁰ K. Lang,³² C. Laughton,¹¹ A. Lebedev,¹² R. Lee,¹² W. Y. Lee,¹⁰ M. A. Libkind,²⁰ J. Ling,²⁸ J. Liu,³² P. J. Litchfield,^{22,26} R. P. Litchfield,²⁴ N. P. Longley,²² P. Lucas,¹¹ W. Luebke,¹³ S. Madani,²⁶ E. Maher,²² V. Makeev,^{11,15} W. A. Mann,³³ A. Marchionni,¹¹ A. D. Marino,¹¹ M. L. Marshak,²² J. S. Marshall,⁶ N. Mayer,²³ J. McDonald,²⁵ A. M. McGowan,^{1,22} J. R. Meier,²² G. I. Merzon,¹⁹ M. D. Messier,^{14,12} R. H. Milburn,³³ J. L. Miller,^{17,14,*} W. H. Miller,²² S. R. Mishra,^{28,12} A. Mislivec,²³ P. S. Miyagawa,²⁴ C. D. Moore,¹¹ J. Morfin,¹¹ R. Morse,³⁰ L. Mualem,²² S. Mufson,¹⁴ S. Murgia,²⁹ M. J. Murtagh,^{4,*} J. Musser,¹⁴ D. Naples,²⁵ C. Nelson,¹¹ J. K. Nelson,^{35,11,22} H. B. Newman,⁵ F. Nezzrick,¹¹ R. J. Nichol,²¹ T. C. Nicholls,²⁶ J. P. Ochoa-Ricoux,⁵ J. Oliver,¹² W. P. Oliver,³³ V. A. Onuchin,¹⁵ T. Osiecki,³² R. Ospanov,³² J. Paley,¹⁴ V. Paolone,²⁵ A. Para,¹¹ T. Patzak,^{9,33} Ž. Pavlović,³² G. F. Pearce,²⁶ N. Pearson,²² C. W. Peck,⁵ C. Perry,²⁴ E. A. Peterson,²² D. A. Petyt,^{22,26,24} H. Ping,³⁶ R. Piteira,⁹ R. Pittam,²⁴ A. Pla-Dalmau,¹¹ R. K. Plunkett,¹¹ L. E. Price,¹ M. Proga,³² D. R. Pushka,¹¹ D. Rahman,²² R. A. Rameika,¹¹ T. M. Rauffer,²⁴ A. L. Read,¹¹ B. Rebel,^{11,14} J. Reichenbacher,¹ D. E. Reyna,¹ C. Rosenfeld,²⁸ H. A. Rubin,¹³ K. Ruddick,²² V. A. Ryabov,¹⁹ R. Saakyan,²¹ M. C. Sanchez,^{12,33} N. Saoulidou,^{11,2} J. Schneps,³³ P. V. Schoessow,¹ P. Schreiner,³ R. Schwienhorst,²² V. K. Semenov,¹⁵ S.-M. Seun,¹² P. Shanahan,¹¹ P. D. Shield,²⁴ W. Smart,¹¹ V. Smirnitsky,¹⁶ C. Smith,^{21,30,5} P. N. Smith,³⁰ A. Sousa,^{24,33} B. Speakman,²² P. Stamoulis,² A. Stefanik,¹¹ P. Sullivan,²⁴ J. M. Swan,²⁰ P. A. Symes,³⁰ N. Tagg,^{33,24} R. L. Talaga,¹ E. Tetteh-Lartey,³¹ J. Thomas,^{21,24,11} J. Thompson,^{25,*} M. A. Thomson,⁶ J. L. Thron,¹ G. Tinti,²⁴ R. Trendler,¹¹ J. Trevor,⁵ I. Trostin,¹⁶ V. A. Tsarev,¹⁹ G. Tzanakos,² J. Urheim,^{14,22} P. Vahle,^{21,32} M. Vakili,³¹ K. Vaziri,¹¹ C. Velissaris,³⁶ V. Verbyusov,¹⁶ B. Viren,⁴ L. Wai,²⁹ C. P. Ward,⁶ D. R. Ward,⁶ M. Watabe,³¹ A. Weber,^{24,26} R. C. Webb,³¹ A. Wehmann,¹¹ N. West,²⁴ C. White,¹³ R. F. White,³⁰ S. G. Wojcicki,²⁹ D. M. Wright,²⁰ Q. K. Wu,²⁸ W. G. Yan,⁸ T. Yang,²⁹ F. X. Yumiceva,³⁵ J. C. Yun,¹¹ H. Zheng,⁵ M. Zois,² and R. Zwaska^{11,32}

(The MINOS Collaboration)

¹Argonne National Laboratory, Argonne, IL 60439

²Department of Physics, University of Athens, GR-15771 Athens, Greece

³Physics Dept., Benedictine University, Lisle, IL 60532

⁴Brookhaven National Laboratory, Upton, NY 11973

⁵Lauritsen Lab, California Institute of Technology, Pasadena, CA 91125

⁶Cavendish Laboratory, Univ. of Cambridge, Madingley Road, Cambridge CB3 0HE, UK

⁷Univ. Estadual de Campinas, IF-UNICAMP, CP 6165, 13083-970, Campinas, SP, Brazil

⁸Inst. of High Energy Physics, Chinese Academy of Sciences, Beijing 100039, China

⁹APC – Collège de France, 11 Place Marcelin Berthelot, F-75231 Paris Cedex 05, France

¹⁰Physics Department, Columbia University, New York, NY 10027

¹¹Fermi National Accelerator Laboratory, Batavia, IL 60510

- ¹²Dept. of Physics, Harvard University, Cambridge, MA 02138
¹³Physics Division, Illinois Institute of Technology, Chicago, IL 60616
¹⁴Physics Department, Indiana University, Bloomington, IN 47405
¹⁵Inst. for High Energy Physics, Protvino, Moscow Region RU-140284, Russia
¹⁶High Energy Exp. Physics Dept., Inst. of Theor. and Exp. Physics, B. Chermushkinskaya, 25, 117218 Moscow, Russia
¹⁷Physics Dept., James Madison University, Harrisonburg, VA 22807
¹⁸Joint Inst. for Nucl. Research, Dubna, Moscow Region, RU-141980, Russia
¹⁹Nuclear Physics Dept., Lebedev Physical Inst., Leninsky Prospect 53, 117924 Moscow, Russia
²⁰Lawrence Livermore National Laboratory, Livermore, CA 94550
²¹Dept. of Physics and Astronomy, University College London, Gower Street, London WC1E 6BT, UK
²²School of Physics and Astronomy, University of Minnesota, Minneapolis, MN 55455
²³Dept. of Physics, Univ. of Minnesota – Duluth, Duluth, MN 55812
²⁴Sub-dept. of Particle Physics, Univ. of Oxford, Denys Wilkinson Bldg, Keble Road, Oxford OX1 3RH, UK
²⁵Dept. of Physics and Astronomy, Univ. of Pittsburgh, Pittsburgh, PA 15260
²⁶Rutherford Appleton Laboratory, Chilton, Didcot, Oxfordshire, OX11 0QX, UK
²⁷Inst. de Física, Univ. de São Paulo, CP 66318, 05315-970, São Paulo, SP, Brazil
²⁸Dept. of Physics and Astronomy, Univ. of South Carolina, Columbia, SC 29208
²⁹Department of Physics, Stanford University, Stanford, CA 94305
³⁰Dept. of Physics and Astronomy, University of Sussex, Falmer, Brighton BN1 9QH, UK
³¹Physics Dept., Texas A&M Univ., College Station, TX 77843
³²Dept. of Physics, Univ. of Texas, 1 University Station, Austin, TX 78712
³³Physics Dept., Tufts University, Medford, MA 02155
³⁴Physics Dept., Western Washington Univ., Bellingham, WA 98225
³⁵Dept. of Physics, College of William & Mary, Williamsburg, VA 23187
³⁶Physics Dept., Univ. of Wisconsin, Madison, WI 53706

(Dated: November 26, 2024)

This letter reports results from the MINOS experiment based on its initial exposure to neutrinos from the Fermilab NuMI beam. The rates and energy spectra of charged current ν_μ interactions are compared in two detectors located along the beam axis at distances of 1 km and 735 km. With 1.27×10^{20} 120 GeV protons incident on the NuMI target, 215 events with energies below 30 GeV are observed at the Far Detector, compared to an expectation of 336 ± 14.4 events. The data are consistent with ν_μ disappearance via oscillations with $|\Delta m_{32}^2| = 2.74_{-0.26}^{+0.44} \times 10^{-3} \text{ eV}^2/c^4$ and $\sin^2(2\theta_{23}) > 0.87$ (68% C.L.).

PACS numbers: 14.60.Lm, 14.60.Pq, 29.27.-a, 29.30.-h

There is now substantial evidence [1, 2, 3, 4, 5, 6, 7, 8] that the proper description of neutrinos involves a rotation between mass and flavor eigenstates governed by the 3×3 PMNS matrix [9, 10]. The parameters of this mixing matrix, three angles and a phase, as well as the mass differences between the three mass eigenstates must be determined experimentally. The Main Injector Neutrino Oscillation Search (MINOS) experiment has been designed to study the flavor composition of a beam of muon neutrinos as it travels between the Near Detector (ND) at Fermi National Accelerator Laboratory at 1 km from the target, and the Far Detector (FD) in the Soudan iron mine in Minnesota at 735 km from the target. From the comparison of the reconstructed neutrino energy spectra at the near and far locations the oscillation parameters $|\Delta m_{32}^2|$ and $\sin^2(2\theta_{23})$ are extracted.

The Neutrinos at the Main Injector (NuMI) neutrino beam is produced using 120 GeV protons from the Main Injector. The protons are delivered in $10 \mu\text{s}$ spills with up to 3.0×10^{13} protons per spill. The extracted protons are bent downward by 3.3° to point at the MINOS detectors. The global positioning system (GPS) defined the survey beam direction to within 12 m of the FD [11]. Pos-

itively charged particles produced by the proton beam in the 95.4 cm long target (mainly π^+ and K^+) are focused by two pulsed parabolic horns spaced 10 m apart and are then allowed to decay in a 675 m long, 2 m diameter, evacuated decay pipe [12]. The proton beam [13] and tertiary muon beam [14] are monitored on a pulse-by-pulse basis. The target position relative to the first horn and the horn current are variable [15]. For the majority of the running period described here, the target was inserted 50.4 cm into the first horn to maximize neutrino production in the 1-3 GeV energy range. A total of 1.27×10^{20} protons on target (POT) were taken in this position and used for the oscillation analysis. The charged current (CC) neutrino event yields at the ND are predicted to be 92.9% ν_μ , 5.8% $\bar{\nu}_\mu$, 1.2% ν_e and 0.1% $\bar{\nu}_e$. The data described here were recorded between May 2005 and February 2006. The average livetime of the FD was 99.0% during this period. About one third of the total ND events provided a sufficiently large dataset for this analysis of $\sim 10^6$ events which were sampled throughout the run period.

Both MINOS detectors [16] are steel-scintillator tracking calorimeters [17] with toroidal magnetic fields averaging 1.3 T [18]. The steel plates are 2.54 cm thick. The

scintillator planes are comprised of 4.1 cm wide and 1 cm thick plastic strips. Each plane is oriented at 45° from vertical and at 90° with respect to its neighbors. The light from the scintillator strips is transported to the multi-anode photomultiplier tubes (PMT) by embedded 1.2 mm diameter wavelength shifting (WLS) fibers. In order to cancel the majority of the uncertainties in the modeling of neutrino interactions and detector response, the two MINOS detectors are as similar as possible. For example, both detectors yield 6 – 7 photoelectrons (PEs) per plane for normally incident minimum ionizing particles. However, the data rate in the ND is $\sim 10^5$ times larger than in the FD which has dictated certain design differences between them.

The 5.4 kton FD, 705 m underground, has 484 octagonal, 8 m wide instrumented planes read out at both ends via Hamamatsu M16 PMTs [19]. Eight WLS fibers from strips in the same plane, separated from each other by about 1 m, are coupled to each pixel. The coupling pattern is different at the two ends to allow resolution of ambiguities.

The 0.98 kton ND, 103 m underground, has 282 irregular $4 \times 6 \text{ m}^2$ octagonal planes. Its geometry optimizes the containment of hadronic showers and provides sufficient flux return to achieve a magnetic field similar to the FD. Each strip is coupled via a WLS fiber to one pixel of a Hamamatsu M64 PMT [20]. The ND readout continuously integrates the PMT charges with a sampling rate of 53.1 MHz to allow discrimination between successive Main Injector RF buckets.

The data acquisition [21, 22, 23] accepts data above a threshold of 0.25 PEs. In the FD, the online trigger conditions require a hit within $100 \mu\text{s}$ centered on the time of the expected beam spill, at least 20 PEs inside a four plane window, or 4 hits in 5 consecutive planes. In the ND, all the data taken during the beam spill are retained. The trigger efficiency for both detectors exceeds 99.5% for neutrino events with visible energy above 0.5 GeV.

The detectors are calibrated using an *in-situ* light injection system [24] and cosmic ray muons. LED generated light signals are distributed to all the WLS fibers to track gain changes in the PMTs and electronics. The energy deposited by through-going muons is used to equalize the response of all the scintillator strips. After calibration, remaining time and position dependent variations in the responses of the detectors result in an uncertainty in the relative energy scale between the two detectors of 2%. The overall energy scale for single hadrons and electrons was determined from the results of a test-beam experiment using a small, unmagnetized copy of the MINOS calorimeters (CalDet) [25]. Stopping muons are then used to relate the results from CalDet to the response of the ND and FD. From these studies, the uncertainty on the absolute hadronic energy scale is estimated to be 6%.

The simulation of the production and detection of neu-

trinos commences with a model of hadron production in the target using FLUKA05 [26], which has uncertainties at the 20-30% level stemming from a lack of relevant thick target hadron production data. The shower products are transported through the horn focusing system and decayed in a GEANT3 [27] simulation that includes the horns, beamline material and the decay pipe. The neutrino event generator, NEUGEN3 [28], is tuned to existing CC cross-section data where present uncertainties below 10 GeV are at the 20% level. The products of the neutrino interaction are propagated out of the iron nucleus using the INTRANUKE [29] code from within NEUGEN3. Some of the energy of absorbed pions is transferred to clusters of nucleons as motivated by Ref. [30]. The response of the detector is simulated using GEANT3 with the GCALOR [31] model of hadronic interactions. The final step in the simulation chain involves photon generation, propagation and transmission through the WLS fiber and conversion to photoelectrons in the PMTs.

In CalDet, GEANT3 with GCALOR is found to reproduce the hadronic and electromagnetic (EM) responses of the detector to single particles to 4% and 2%, respectively. Below 10 GeV, the hadronic energy resolution was measured to be $56\%/\sqrt{E[\text{GeV}]} \oplus 2\%$ [32] and the EM resolution was measured to be $21.4\%/\sqrt{E[\text{GeV}]} \oplus 4.1\%/E[\text{GeV}]$ [33]. The muon energy resolution $\Delta E_\mu/E_\mu$ varies smoothly from 6% for E_μ above 1 GeV where most tracks are contained and measured by range, to 13% at high energies, where the curvature measurement is primarily used.

The initial step in the reconstruction of the FD data is the removal of the eightfold hit-to-strip ambiguity using information from both strip ends. In the ND, timing and spatial information is first used to separate individual neutrino interactions from the same spill. Subsequently, tracks are found and fitted, and showers are reconstructed, in the same way in both detectors. For ν_μ CC events, the total reconstructed event energy is obtained by summing the muon energy and the visible energy of the hadronic system.

The FD data set was left blind until the selection procedure had been defined and the prediction of the unoscillated spectrum was understood. The blinding procedure hid a substantial fraction of the FD events with the precise fraction and energy spectrum of the hidden sample unknown. Events are pre-selected in both detectors, by requiring total reconstructed energy below 30 GeV and a negatively charged track to suppress events that originate from π^- or K^\pm . The track vertex must be within a fiducial volume such that cosmic rays are rejected and the hadronic energy of the event is contained within the volume of the detector. The event time must fall within a $50 \mu\text{s}$ window around the spill time. Cosmic ray background is suppressed further in the FD by requiring the track to point within 53° of the neutrino beam direc-

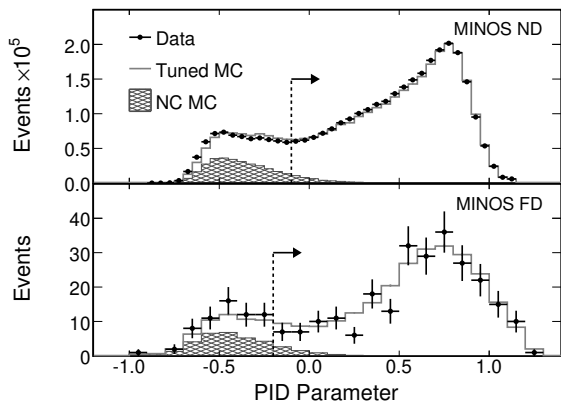


FIG. 1: Data and tuned MC predictions for the PID variable in the ND (top) and FD (bottom). The arrows depict the positions of the ND and FD selection cuts. The FD MC distribution for CC events uses the best fit parameters discussed in the text.

tion. The pre-selected ν_μ event sample is predominantly CC with a 8.6% NC background estimated from Monte Carlo (MC) simulations. The fiducial mass of the FD (ND) is 72.9% (4.5%) of the total detector mass.

A particle identification parameter (PID) incorporating probability density functions for the event length, the fraction of energy contained in the track and the average track pulse height per plane provides separation of ν_μ CC and NC events. The PID is shown in Fig. 1 for ND and FD data overlaid with simulations of NC and CC events after the beam reweighting procedure described below. Events with PID above -0.2 (FD) and -0.1 (ND) are selected as being predominantly CC in origin. These values were optimized for both detectors such that the resulting purity of each sample is about 98%. The efficiencies for selecting ν_μ CC events in the fiducial volume with energy below 30 GeV are 74% (FD) and 67% (ND). From the absence of any events less than $20 \mu\text{s}$ before and less than $30 \mu\text{s}$ after the spill time, the remaining non-beam related background in the FD is estimated to be less than 0.5 events (68% C.L.). Background from ν_μ interactions in the rock surrounding the FD is estimated from MC to be below 0.4 (68% C.L.) events. The corresponding backgrounds in the ND are negligible.

To constrain hadron production, a series of six runs of similar exposure was taken where the position of the target and the magnitude of the horn magnetic field were varied. Comparisons of the ND energy spectra with MC simulations, shown in Fig. 2, showed an energy dependent discrepancy that changed with the beam settings. This implied beam modeling, rather than detector or cross-section effects, was the primary cause. To bring the MC into better agreement with the data, a tuning of the beam MC was performed in which pion production off the target was smoothly varied in transverse and longitudinal momentum with respect to the FLUKA05 input, as was the overall kaon yield. In addition, the potential sys-

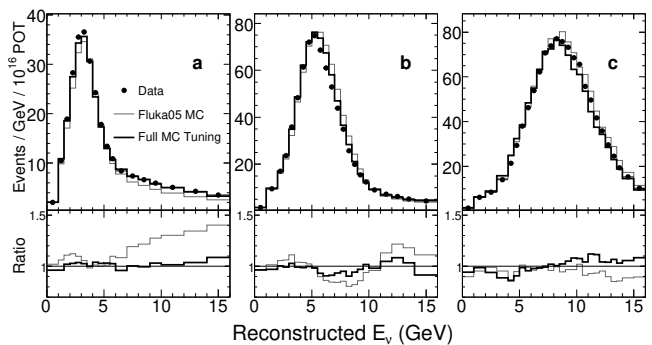


FIG. 2: Energy spectra in the MINOS ND for three of the six beam configurations before and after the 15 parameter beam tuning procedure. The target location was modified to produce the different spectra: a) nominal, b) target at 90 cm from nominal, c) target at 240 cm from nominal. The lower inset shows the ratio of data to MC before and after tuning.

tematic effects of the beam focusing, NC background, ν_μ energy scale and offset were allowed to vary. All of these parameters were found to lie within two standard deviations of their nominal values. Fig. 2 shows the effect of the full beam parameter tuning for the spectra corresponding to three different target positions. The resulting agreement is improved in all beams across the 1-30 GeV neutrino energy region.

The measurement of the energy spectrum at the ND is used to predict the unoscillated spectrum at the FD. The oscillation hypotheses are then tested relative to this prediction. The prediction must take into account the ND and FD spectral differences that are present, even in the absence of oscillations, due to pion decay kinematics and beamline geometry. These introduce a ND/FD shape difference of up to $\sim 20\%$ on either side of the peak.

There are two distinct approaches to the beam extrapolation. The *ND Fit* method focuses on minimizing the remaining ND data and MC differences by modifying MC parameters associated with neutrino interactions and detector response. The FD MC is then re-weighted with the best-fit values of these parameters. For the results presented in this paper, the *Beam Matrix* method [34] is used, in which agreement between MC and data is much less important because the ND data are used to measure all the effects common to both detectors, such as beam modeling, neutrino interactions and detector response. It utilizes the beam simulation to derive a transfer matrix that relates ν_μ s in the two detectors via their parent hadrons. The matrix element M_{ij} gives the relative probability that the distribution of secondary hadrons which produce ν_μ s of energy E_i in the ND will give ν_μ s of energy E_j in the FD. The ND reconstructed event energy spectrum is translated into a flux by first correcting for the simulated ND acceptance and then dividing by the calculated cross-sections for each energy bin. This flux is multiplied by the matrix to yield the predicted,

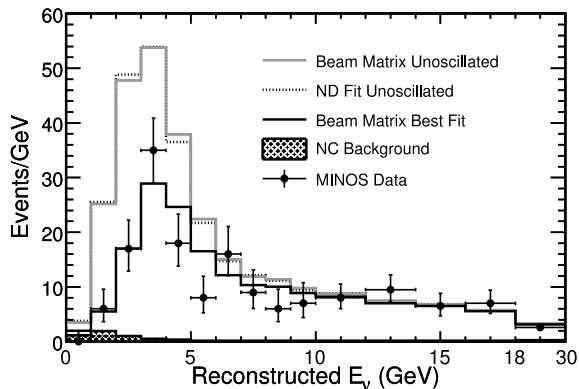


FIG. 3: Comparison of the Far Detector spectrum with predictions for no oscillations for both analysis methods and for oscillations with the best-fit parameters from the Beam Matrix extrapolation method. The estimated NC background is also shown. The last energy bin contains events between 18-30 GeV.

unoscillated FD flux. After the inverse correction for cross-section and FD acceptance, the predicted FD visible energy spectrum is obtained.

In total, 215 events are observed below 30 GeV compared to the unoscillated expectation of 336.0 ± 14.4 . The error is due to the systematic uncertainties described below. In the region below 10 GeV, 122 events are observed compared to the expectation of 238.7 ± 10.7 . The observed energy spectrum is shown along with the predicted spectra for both extrapolation methods in Fig. 3.

Under the assumption that the observed deficit is due to $\nu_\mu \rightarrow \nu_\tau$ oscillations [35, 36, 37], a fit is performed to the parameters $|\Delta m_{32}^2|$ and $\sin^2(2\theta_{23})$ using the expression for the ν_μ survival probability:

$$P(\nu_\mu \rightarrow \nu_\mu) = 1 - \sin^2(2\theta_{23}) \sin^2(1.27 \Delta m_{32}^2 \frac{L}{E}) \quad (1)$$

where L [km] is the distance from the target, E [GeV] is the neutrino energy, and $|\Delta m_{32}^2|$ [38] is measured in eV^2/c^4 . The FD data are binned in reconstructed event energy and the observed number of events in each bin is compared to the expected number of events for this oscillation hypothesis. The best fit parameters are those which minimize $\chi^2 = -2 \ln \lambda$ where λ is the likelihood ratio:

$$\chi^2 = \sum_{n \text{ bins}} (2(e_i - o_i) + 2o_i \ln(o_i/e_i)) + \sum_{n \text{ sys}} \frac{\Delta s_j^2}{\sigma_{s_j}^2} \quad (2)$$

where o_i and e_i are the observed and expected numbers of events in bin i , and the $\Delta s_j^2/\sigma_{s_j}^2$ are the penalty terms for nuisance parameters associated with the systematic uncertainties. The expected number of events depends on $|\Delta m_{32}^2|$, $\sin^2(2\theta_{23})$ and the s_j . The choice of these systematic effects and their estimated uncertainties are described below. The e_i include the small contribution

from selected ν_τ events produced in the oscillation process.

The effects of different systematic uncertainties were evaluated by modifying the MC and performing a fit on this in place of the data. The differences between the fitted values obtained with the modified and unmodified MC are listed in Table I. The largest effects are: (a) The uncertainty in the fiducial mass in both detectors, uncertainty in the event selection efficiency and the POT counting accuracy gives a 4% uncertainty on the predicted FD event rate. (b) The absolute hadronic energy scale from a combination of test beam measurements and calibration accuracy is known to 6% as discussed above. This is added in quadrature to the uncertainty in the effect of intra-nuclear re-scattering estimated at $\pm 10\%$ of the hadronic energy. The total hadronic energy scale uncertainty is therefore $\pm 11\%$. (c) The NC component was varied in a fit to the PID data distribution in six energy bins in the ND. A 50% uncertainty was estimated to encompass the differences between the fit and NC MC. At the current level of statistics, uncertainties from CC cross-sections, muon momentum, relative ND/FD energy calibration, remaining beam uncertainties and reconstruction were found to be negligible. As an example, in the absence of any beam tuning, the best fit value only shifts by $0.2 \times 10^{-5} \text{eV}^2/c^4$.

In fitting the data to Eqn. 1, $\sin^2(2\theta_{23})$ was constrained to lie in the physical region and the main systematic uncertainties ((a), (b) and (c) in Table I) were included as the nuisance parameters. The resulting 68% and 90% confidence intervals are shown in Fig. 4 as determined from $\Delta\chi^2 = 2.3$ and 4.6, respectively [39]. The best fit value for $|\Delta m_{32}^2|$ is $|\Delta m_{32}^2| = (2.74_{-0.26}^{+0.44}) \times 10^{-3} \text{eV}^2/c^4$ and $\sin^2(2\theta_{23}) > 0.87$ at 68% C.L. [40] with a fit probability of 8.9%. At 90% C.L. $(2.31 < |\Delta m_{32}^2| < 3.43) \times 10^{-3} \text{eV}^2/c^4$, and $\sin^2(2\theta_{23}) > 0.78$. The data and best fit MC are shown in Fig. 3. At the best fit value, the MC predicts 0.76 ν_τ events in the final sample. If the fit is not constrained to be within the physical region, $|\Delta m_{32}^2| = 2.72 \times 10^{-3} \text{eV}^2/c^4$ and $\sin^2(2\theta_{23}) = 1.01$, with a 0.2 decrease in χ^2 . With additional data, it is expected that the systematic uncertainties will be reduced.

This work was supported by the US DOE; the UK PPARC; the US NSF; the State and University of Minnesota; the University of Athens, Greece and Brazil's FAPESP and CNPq. We are grateful to the Minnesota Department of Natural Resources, the crew of the Soudan Underground Laboratory, and the staff of Fermilab for their contribution to this effort.

* Deceased.

[1] Y. Ashie et al., Phys. Rev. Lett. 93, 101801 (2004).
[2] Y. Ashie et al., Phys. Rev. D71, 112005 (2005).

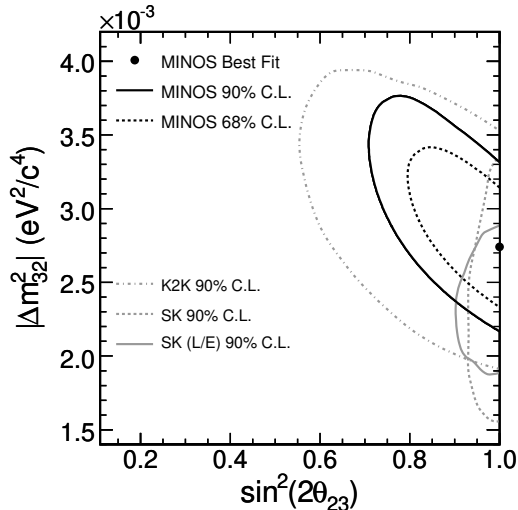


FIG. 4: Confidence intervals for the fit using the Beam Matrix method including systematic errors. Also shown are the contours from the previous highest precision experiments [1, 2, 5].

Uncertainty	$ \Delta m_{32}^2 $ ($10^{-3} \text{ eV}^2/c^4$)	$\sin^2(2\theta_{23})$
(a) Normalization ($\pm 4\%$)	0.05	0.005
(b) Abs. hadronic E scale ($\pm 11\%$)	0.06	0.048
(c) NC contamination ($\pm 50\%$)	0.09	0.050
All other systematics	0.04	0.011

TABLE I: Sources of systematic uncertainties in the measurement of $|\Delta m_{32}^2|$ and $\sin^2(2\theta_{23})$. The values of $|\Delta m_{32}^2|$ and $\sin^2(2\theta_{23})$ used in the systematic MC study were the best fit values from the data. The values are the average shifts for varying the parameters in both directions without imposing constraints on the fit. Correlations between the systematic effects are not taken into account.

- [3] W.W.M. Allison et al., Phys. Rev. D72, 052005 (2005).
- [4] M. Ambrosio et al., Eur. Phys. J. C36, 323 (2004).
- [5] E. Aliu et al., Phys. Rev. Lett. 94, 081802 (2005).
- [6] J. Hosaka et al., Phys. Rev. D73, 112001 (2006).
- [7] S.N. Ahmed et al., Phys. Rev. Lett. 92, 181301 (2004).
- [8] T. Araki et al., Phys. Rev. Lett. 94, 081801 (2005).
- [9] B. Pontecorvo, JETP (USSR) 34, 247 (1958).
- [10] Z. Maki, M. Nakagawa, and S. Sakata, Prog. Theor. Phys. 28, 870 (1962).

- [11] V. Bocean, Proc. 6th Int. Workshop on Acc. Alignment, IWAA99, Grenoble, France (1999).
- [12] A.G. Abramov et al., Nucl. Instrum. & Meth. A485, 209 (2002).
- [13] D. Indurthy et al., Fermilab-Conf-04-520-AD (2004).
- [14] S. Kopp et al, Fermilab-Pub-06-007-AD (2006). Accepted by Nucl. Inst. & Meth.
- [15] M. Kostin et al., Fermilab-TM-2353-AD (2001).
- [16] D.G. Michael et al., The MINOS Detectors, to be submitted to Nucl. Inst. & Meth.
- [17] P. Adamson et al., IEEE Trans. Nucl. Sci. 49, 861 (2002).
- [18] J.K. Nelson, Int. J. Mod. Phys. A16 Suppl O1C, 1181 (2001).
- [19] K. Lang et al., Nucl. Inst. & Meth. A545, 853 (2005).
- [20] N. Tagg et al., Nucl. Inst. & Meth. A539, 668 (2005).
- [21] A. Belias et al., IEEE Trans. Nucl. Sci. 51, 451 (2004).
- [22] J. Oliver et al., IEEE Trans. Nucl. Sci. 51, 2193 (2004).
- [23] T. Cundiff et al., IEEE Trans. on Nucl. Sci., 53, 1347 (2006).
- [24] P. Adamson et al., Nucl. Inst. & Meth. A492, 325 (2002) and A521, 361 (2004).
- [25] P. Adamson et al., Nucl. Inst. & Meth. A556, 119 (2006).
- [26] A. Fasso et al., CERN-2005-10, INFN/TC_05/11, SLAC-R-773 (2005).
- [27] R. Brun et al., CERN DD/EE/84-1 (1984).
- [28] H. Gallagher, Nucl. Phys. B (Proc. Suppl.) 112, 188 (2002).
- [29] R. Merenyi et al., Phys. Rev. D45 743 (1992).
- [30] R.D. Ransome, Nucl. Phys. Proc. Suppl. 139 208 (2005).
- [31] T.A. Gabriel et al., Nucl. Inst. & Meth A349, 106 (1994).
- [32] M. Kordosky, Ph.D. Thesis, UT Austin (2004).
- [33] P. Vahle, Ph.D. Thesis, UT Austin (2004).
- [34] M. Szleper and A. Para, hep-ex/0110001.
- [35] M. Apollonio et al., Eur. Phys. J. C27, 331 (2003).
- [36] F. Boehm et al., Phys. Rev. D64, 112001 (2001).
- [37] M. H. Ahn et al., Phys. Rev. Lett. 93, 051801 (2004).
- [38] The experiment measures an unresolved mixture of $|\Delta m_{31}^2|$ and $|\Delta m_{32}^2|$, which we refer to as $|\Delta m_{32}^2|$ for brevity. For further discussion see G. L. Fogli et al., Prog. Part. Nucl. Phys. 57, 742 (2006).
- [39] The effect of the constraint to the physical region was investigated using the unified approach of G.J. Feldman and R.D. Cousins, Phys. Rev. D57, 3873, (1998), which gave slightly smaller confidence intervals.
- [40] Although the contours in Fig. 4 are calculated with two degrees of freedom (DoF), the parameter errors are calculated with only one DoF as in W.-M. Yao et al., J. Phys. G 33, 1 (2006).